Surpporting Information

Cage-Structured M_xP_y@CNCs (M=Co and Zn) from MOFs Confined Growth in Carbon Nanocages for Superior Lithium Storage and Hydrogen Evolution Performance

Wenlong Li[a†], Rongfang Zhao[b†], Kehan Zhou[a], Chao Shen[a], Xiue Zhang[a], Huayu Wu[a], Lubin Ni[a], Hui Yan[c]*, Guowang Diao[a], Ming Chen[a]*

[a]School of Chemistry and Chemical Engineering, Yangzhou University, Yangzhou, 225002, Jiangsu, China

[b]Yantai Institute of Coastal Zone Research, Chinese Academy of Sciences, Yantai 264003, Shandong, China

[c]Department of Chemistry, University of Louisiana at Lafayette, Lafayette, LA 70504, United States of America

Experimental Section

Materials characterization

Field-emission scanning electron microscopy (FESEM) was carried out with Hitachi S-4800 (Japan). Transmission Electron Microscopy (TEM) was conducted on JEOL JEM-2100 instrument. High-resolution TEM (HRTEM) and high-angle annular dark-field scanning transmission electron microscopy (HAADF-STEM) were performed on FEI Tecnai G2 F30 STWIN (USA) operating at 300 kV. X-ray diffraction (XRD) data were obtained with a graphite monochromator and Cu Kα radiation (λ= 0.1541 nm) on D8 advance superspeed powder diffractometer (Bruker). Raman spectra were carried out on Renishaw via Raman spectroscope. X-ray photoelectron spectroscopy (XPS) were conducted by Thermo Escalab 250 system using Al Ka radiation (hv = 1486.6 eV), the pressure of test chamber was maintained below 2×10^{-9} Torr during spectral acquisition. Thermogravimetry analysis (TGA, Pyris 1 TGA, PerkinElmer, USA) data were obtained in air. Surface areas and pore size distributions were recorded by BET technique in an automated surface area and porosity analyzer (ASAP 2020, HD88) at -196 ^{o}C after samples being dried at 100 ^{o}C for 4 h .

Synthesis of carbon nanocages

Ethanol (75 ml), deionized water (10 ml) and ammonia (3 ml) were mixed, then 3.46 ml of tetraethylorthosilicate (TEOS) was added into the mixture drop by drop at room temperature. The solution was stirred at room temperature for 10 min to form SiO_2 nanospheres. Next, 0.56 ml resorcinol and 0.4 g formaldehyde solution were added to the above reaction system, and the mixture was mechanically stirred for 24 h at room temperature. After centrifugation and washing, the solid was dried at 60° C for 12 h to form SiO_2@SiO_2/resorcinol-formaldehyde resin (RF); the

dried SiO_2@SiO_2/RF was thencalcined at 700 °C for 5 h in an argon atmosphere, and the heating rate was 2 °C min^{-1}, to obtain SiO_2@ SiO_2/C spheres.

The calcined SiO_2@ SiO_2/C spheres were dispersed in 50 ml 1 M sodium hydroxide aqueous solution and etched at 80 °C for 2 h. After completion of the reaction, the solid phase was washed by water and ethanol for three times, and then dried at 60 °C to form hollow mesoporous carbon spheres, named as carbon nanocages (CNCs).

Synthesis of nanocage structured MOFs@CNCs

CNCs were dispersed in 25 ml methanol solution. After homogeneous dispersion, 291 mg $Co(NO_3)_2 \cdot 6H_2O$ (1 mmol) , and 328 mg 2-methylimidazole (4 mmol) were added into CNCs/methanol solution. At the end of the reaction, the solid mixture was separated and washed by water and ethanol for three times, separated by centrifugation, and then dried at 60 °C for 12 hours to obtain nanocage structured ZIF-67@CNCs.

The confined growth of ZIF-8 in CNCs followed the same procedure as that of ZIF-67 by replacing $Co(NO_3)_2 \cdot 6H_2O$ with 297 mg $Zn(NO_3)_2 \cdot 6H_2O$ (1 mmol).

Synthesis of M_xP_y@CNCs

In the synthesis of a typical CoP hybrid composite, ZIF-67@CNCs and red phosphorus were placed on both sides of the quartz boat at a mass ratio of 1:1, and then the mixture was heated to 800 °C in Ar. Incubation in a high purity argon atmosphere for 2 h gave nanocage-structured CoP@CNCs.

The nanocage structured ZnP_4@CNCs were obtained by annealing ZIF-8@CNCs and NaH_2PO_4, a mass ratio of 1:5 at 500 ^oC for 2 hours, with a ramping rate of 2 °C min^{-1} under argon.

Electrochemical tests

Anode electrodes were prepared by mixing the CoP@CNCs or ZnP_4@CNCs nanocages (80%) with 10 % acetylene black as a conductive material, and 10 % polyvinylidene difluoride (PVDF) binder dissolved in N-methyl-2-pyrrolidinone (NMP). Then, the slurries were cast onto a copper foil current collector. After coating, the electrodes were dried at 80 °C for 10 h to remove the solvent before pressing. The electrodes were punched in the form of disks and then vacuum-dried at 120 °C for 12 h. And then the button cells (CR 2032 coin-type cell) were assembled with metallic lithium as the counter/reference electrode, 1 M $LiPF_6$ in EC/DMC/EMC (1:1:1 by volume) is used as electrolyte, and Celgard 2400 polypropylene as separator in a high-purity argon-filled glovebox (Vacuum Atmospheres Co., Ltd).

Cyclic voltammetry (CV) measurements were performed using an electrochemical workstation (CHI660 E, Chenghua, CHN) at a scan rate of 0.1 mV s^{-1} between 0.001 and 3.0 V. Electrochemical impedance spectroscopic (EIS) experiments were performed with Autolab Electrochemical Analyzer (Ecochemie, Netherlands). Galvanostatic charge (lithium insertion) and discharge (lithium extraction) cycles of the cells were carried out using a battery test system (CT-3008W, Xinwei, CHN) at various current densities between 0.001 and 3 V (*vs.* Li^+/Li) to determine rate performance, and to evaluate cycle stability at the current density of 0.5 A g^{-1}.

Supplementary Figures Captions

Figure S1 SEM (a, c, e) and TEM (b, d, f)images of (a)(b) SiO_2@SiO_2/RF nanospheres, (c)(d) SiO_2@SiO_2/C nanospheres, and (e)(f) carbon nanocages.

Figure S2 FTIR spectra of ZIF-67 and ZIF-67@CNCs.

Figure S3 XRD spectra of ZIF-67 and ZIF-67@CNCs.

Figure S4 (a-b) SEM, (c) TEM images of ZIF-67.

Figure S5 HRTEM image of CoP@CNCs.

Figure S6 (a-b) SEM, (c) TEM images of CoP/C-N.

Figure S7 TGA curves of CoP@CNCs.

Figure S8 (a) SEM and (b) TEM images of ZIF-8.

Figure S9 (a) SEM, (b) TEM images of ZnP_4/C-N.

Figure S10 TGA curves of ZnP_4@CNCs.

Figure S11 XPS survey scan and high resolution spectrum (C1s) of CoP@CNCs.

Figure S12 XPS survey scan and high resolution spectrum (C1s) ZnP_4@CNCs.

Figure S13 XPS survey scan and high resolution spectrum (C1s) of CNCs and C1s.

Figure S14 XPS survey scan (a) CNCs, and high resolution spectrum: (b) C 1s and (c) P 2p.

Figure S15 Zeta potential of CNCs, CNCs/Co^{2+}, and CNCs/Zn^{2+}.

Figure S16 FT-IR spectra of CNCs, CNCs/Co^{2+}, and CNCs/Zn^{2+}.

Figure S17 Cycling performance at various current densities of CNCs.

Figure S18 Cycling performance and Coulombic efficiency of CNCs at 1A g^{-1}.

Figure S19 Cycling performance at various current densities of ZIF-67@CNCs.

Figure S20 Cycling performance at various current densities of ZIF-8@CNCs.

Figure S21 TEM and HRTEM images of (a) CoP@CNCs and (b) ZnP_4@CNCs after 200 cycles at 2 A g^{-1}.

Table S1 Summary of electrochemical performances of different CoP_x-based or ZnP_x-based anodes.

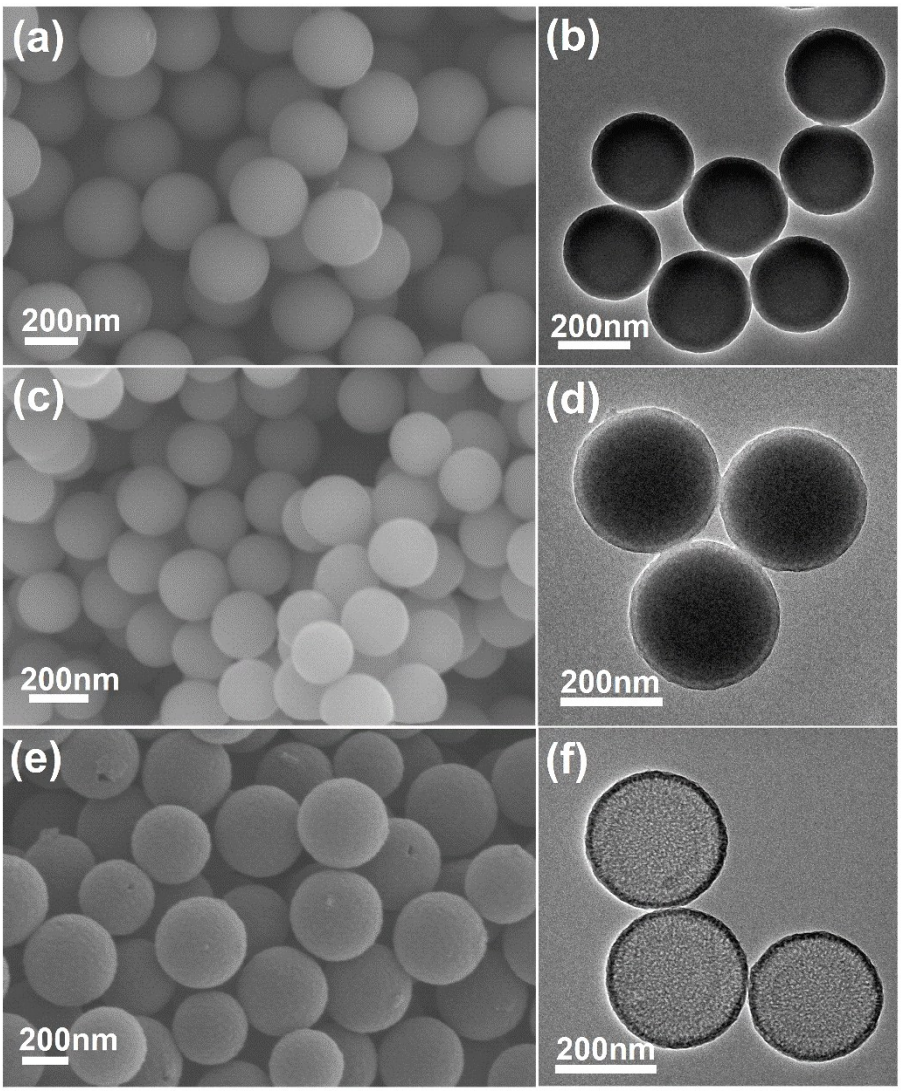

Figure S1 SEM (a, c, e) and TEM (b, d, f)images of (a)(b) SiO_2@SiO_2/RF nanospheres, (c)(d) SiO_2@SiO_2/C nanospheres, and (e)(f) carbon nanocages.

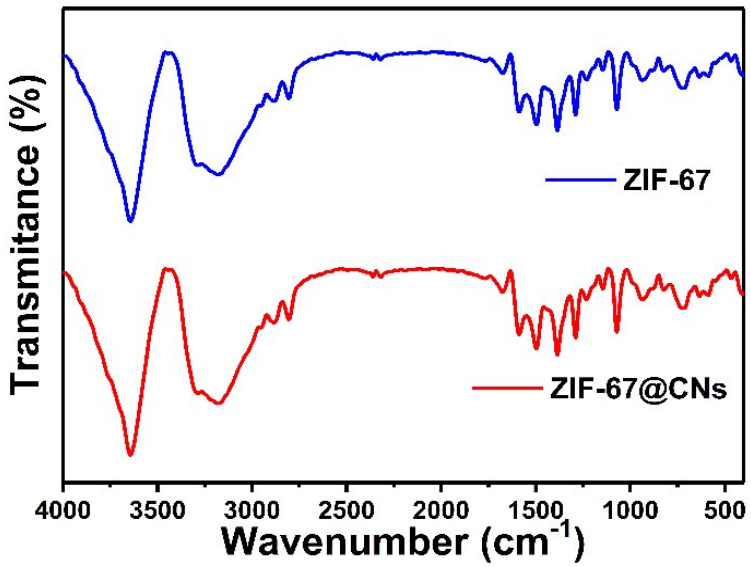

Figure S2 FTIR spectra of ZIF-67 and ZIF-67@CNCs.

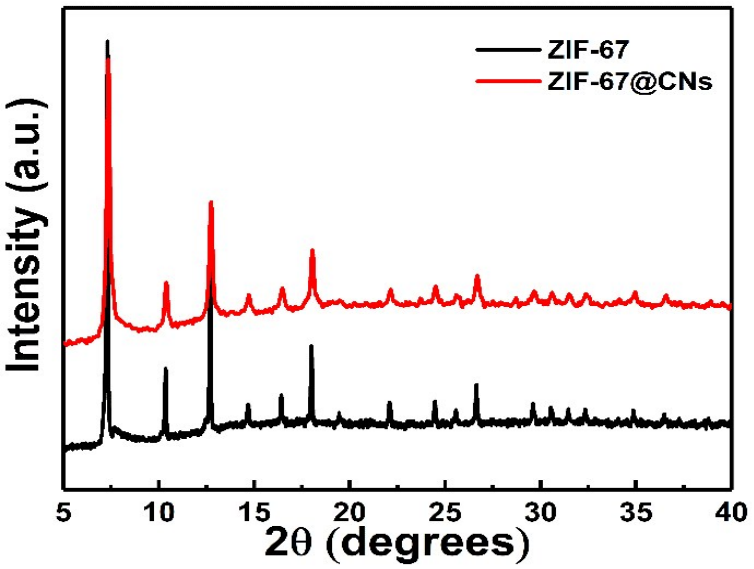

Figure S3 XRD spectra of ZIF-67 and ZIF-67@CNCs.

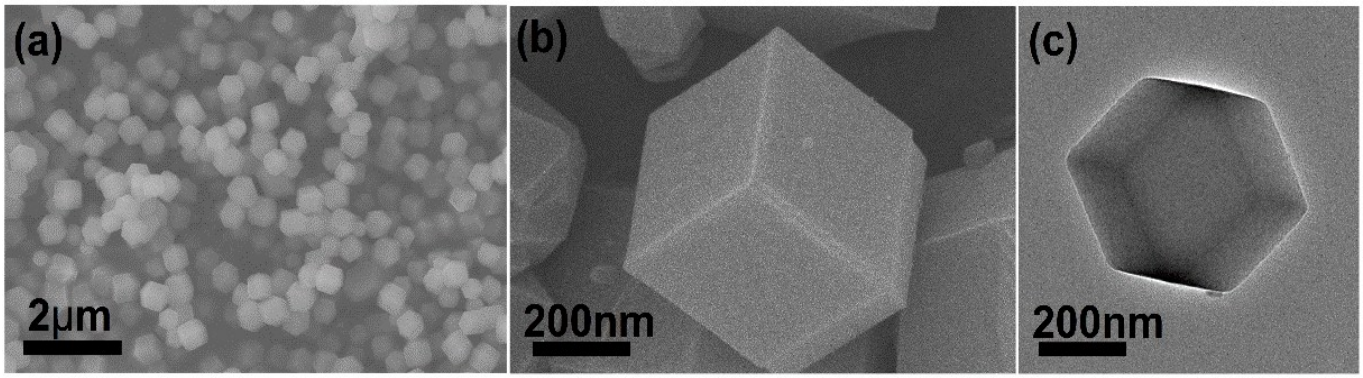

Figure S4 (a-b) SEM, (c) TEM images of ZIF-67.

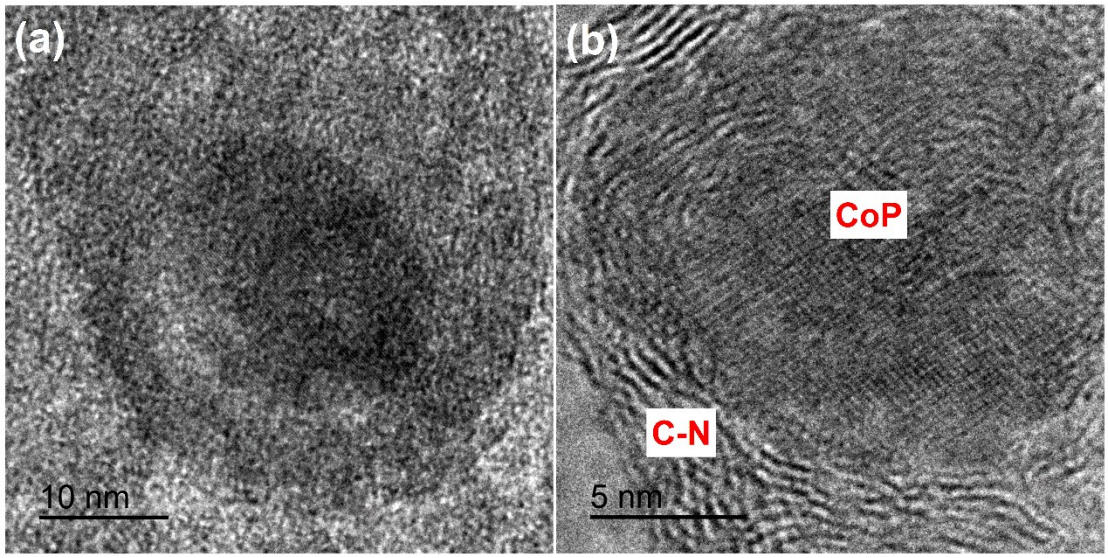

Figure S5 HRTEM image of CoP@CNCs.

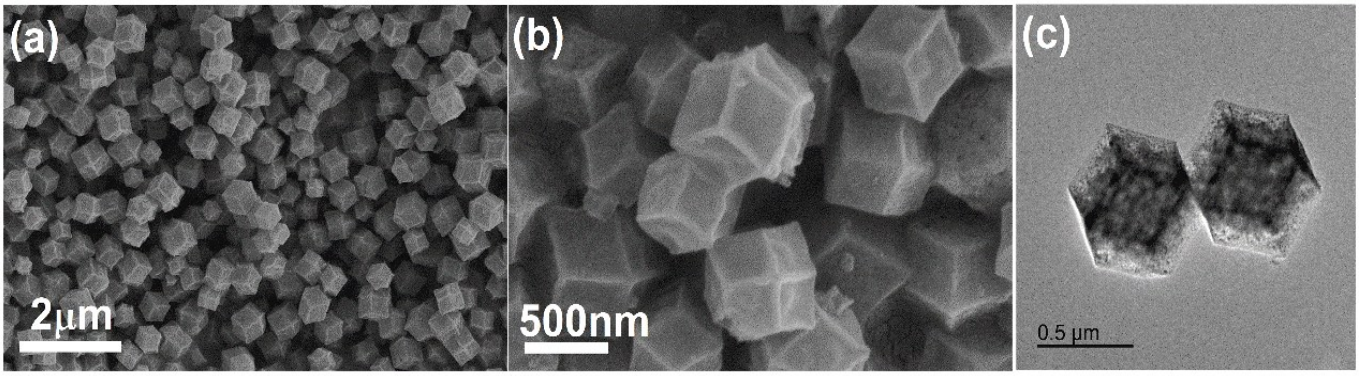

Figure S6 (a-b) SEM, (c) TEM images of CoP/C-N.

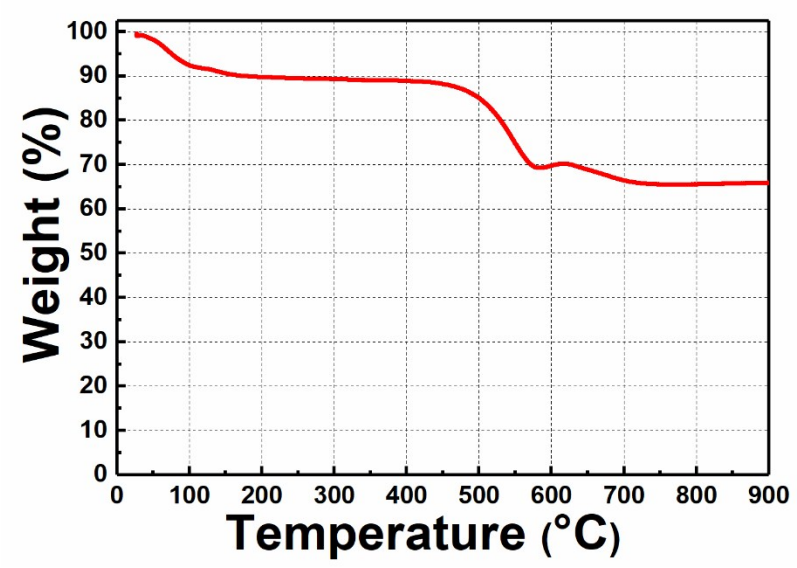

Figure S7 TGA curves of CoP@CNCs.

For CoP@CNCs, the weight loss is two stages. First, when the temperature is lower than 150 °C, water or other inactive substance left. Second, when the temperature reaches about 500 °C, carbon and phosphorus elements start to turn into gaseous substance. At 570 °C, the weight is increased slightly, which might be attributed to the formation of Co_3O_4. Finally, the residual, Co_3O_4, weight percentage content is 64.50%.

The mass percentage content of CoP is calculated by the formula:

$$w\%(M_xP_y) = A\% \times \frac{M(CoP)}{M(Co_3O_4)} \times \frac{1}{(1 - B\%)} \times 100\% \quad (1)$$

Where $A\%$ is the residual weight percentage content; $B\%$ is the water or other inactive substance weight percentage content;

According the equation, the mass percentage content of CoP in the hybrid of CoP@CNCs is 80.89wt.%.

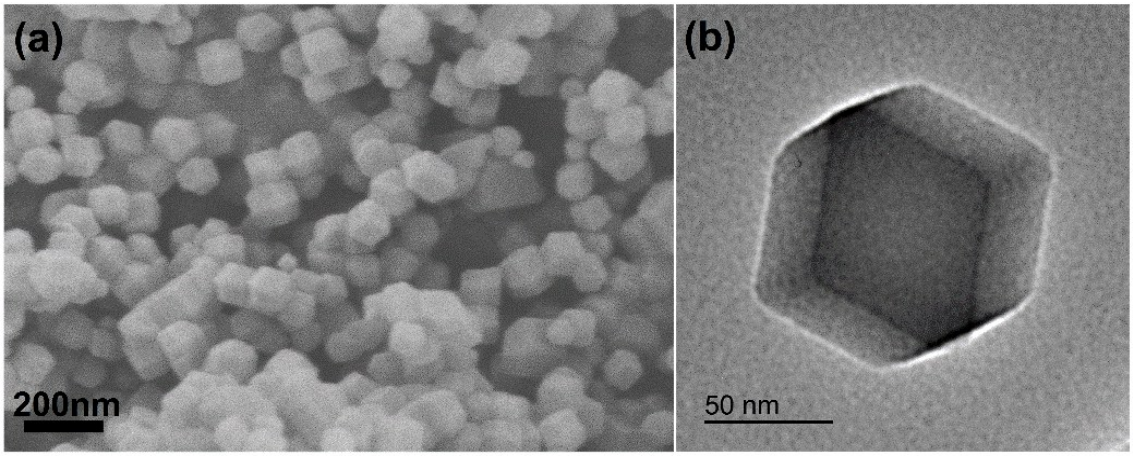

Figure S8 (a) SEM and (b) TEM images of ZIF-8.

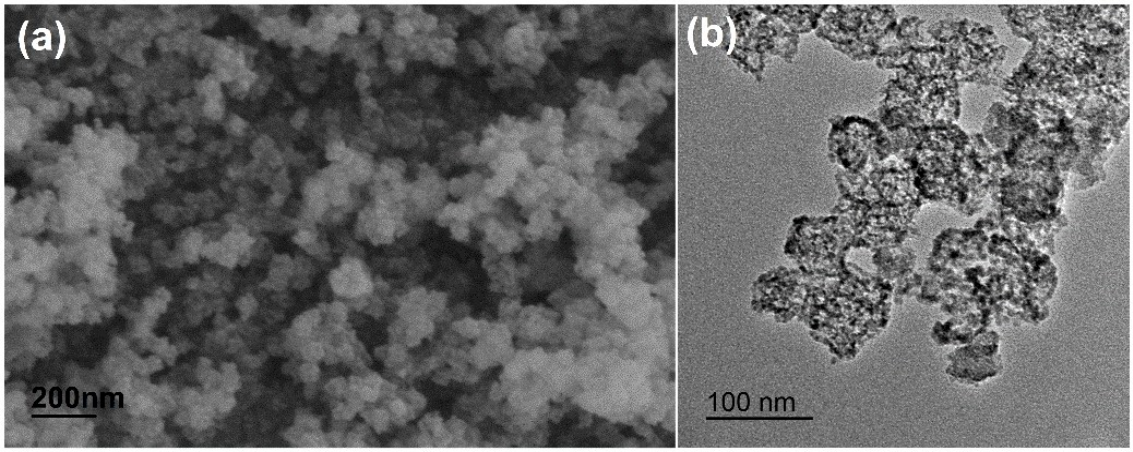

Figure S9 (a) SEM, (b) TEM images of ZnP_4/C-N.

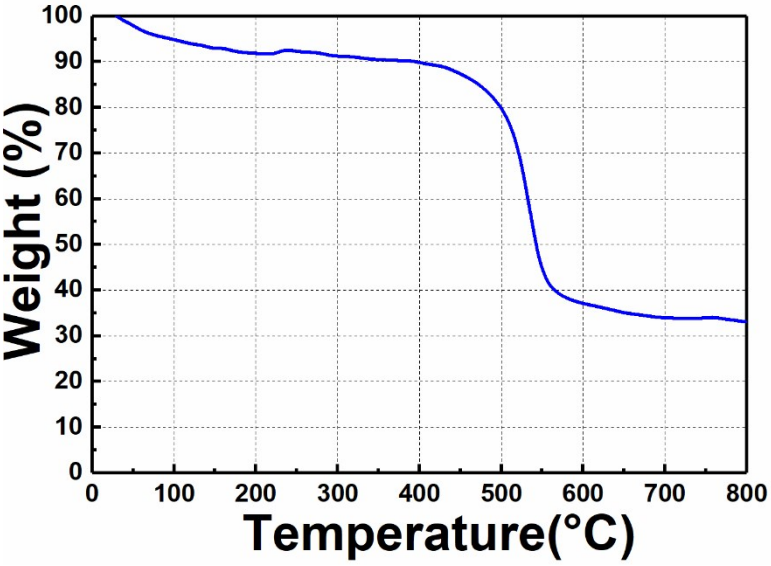

Figure S10 TGA curves of ZnP_4@CNCs.

For ZnP_4@CNCs, carbon and phosphorus elements will turn into gaseous substance and the final residue is ZnO. The weight loss of ZnP_4@CNCs is similar to that of CoP@CNCs. When the temperature reach about 500 °C, carbon and phosphorus elements start to turn into gaseous substance. Finally, the residual weight percentage content is 33.00%.

The mass percentage content of ZnP_4 is calculated by the formula:

$$w\%(\mathrm{M_xP_y}) = A\% \times \frac{M(\mathrm{ZnP4})}{M(\mathrm{ZnO})} \times \frac{1}{(1 - B\%)} \times 100\% \quad (2)$$

Where A% is the residual weight percentage content; B% is the water or other inactive substance weight percentage content;

According the equation 2, the mass percentage content of ZnP_4 in the hybrid of ZnP_4@CNCs equals 85.25 wt.%.

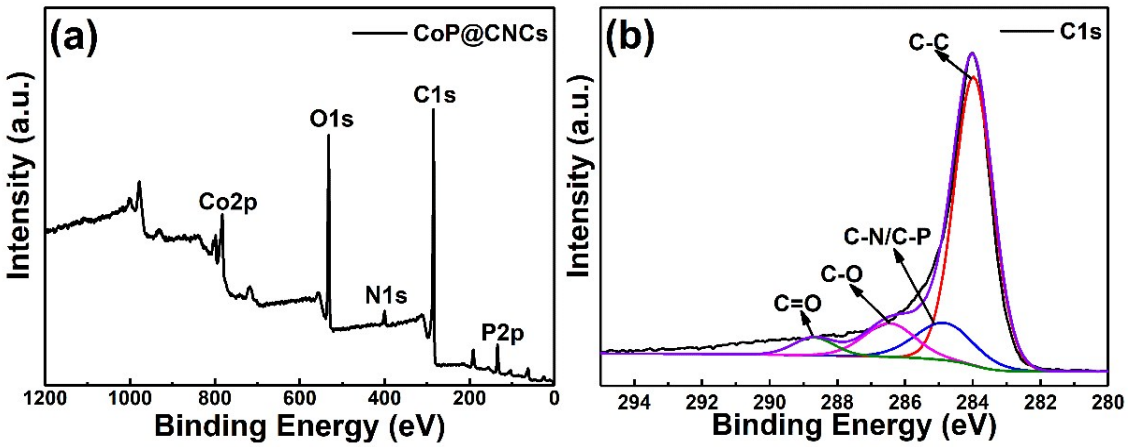

Figure S11 XPS survey scan and high resolution spectrum (C1s) of CoP@CNCs.

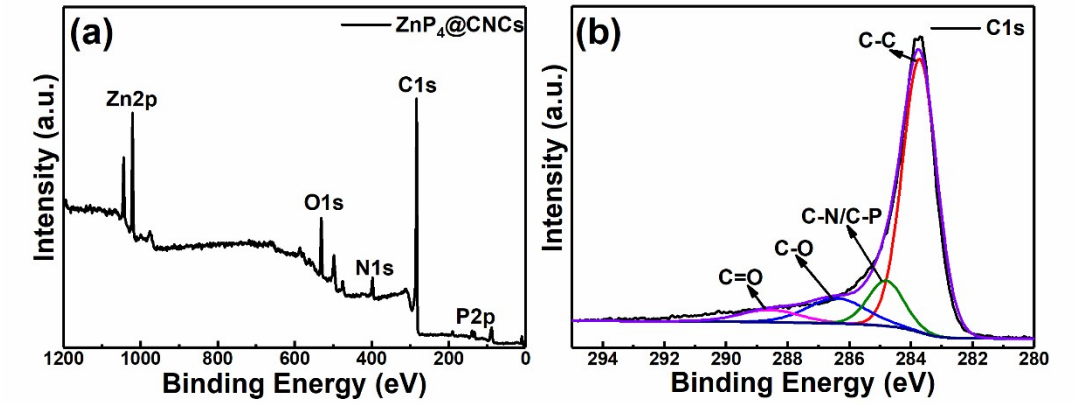

Figure S12 XPS survey scan and high resolution spectrum (C1s) ZnP_4@CNCs.

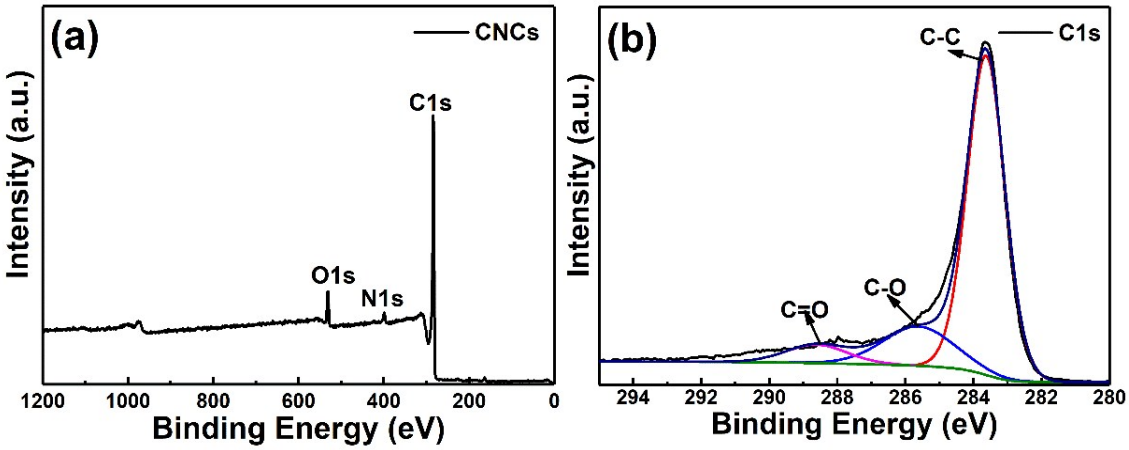

Figure S13 XPS survey scan and high resolution spectrum (C1s) of CNCs and C1s.

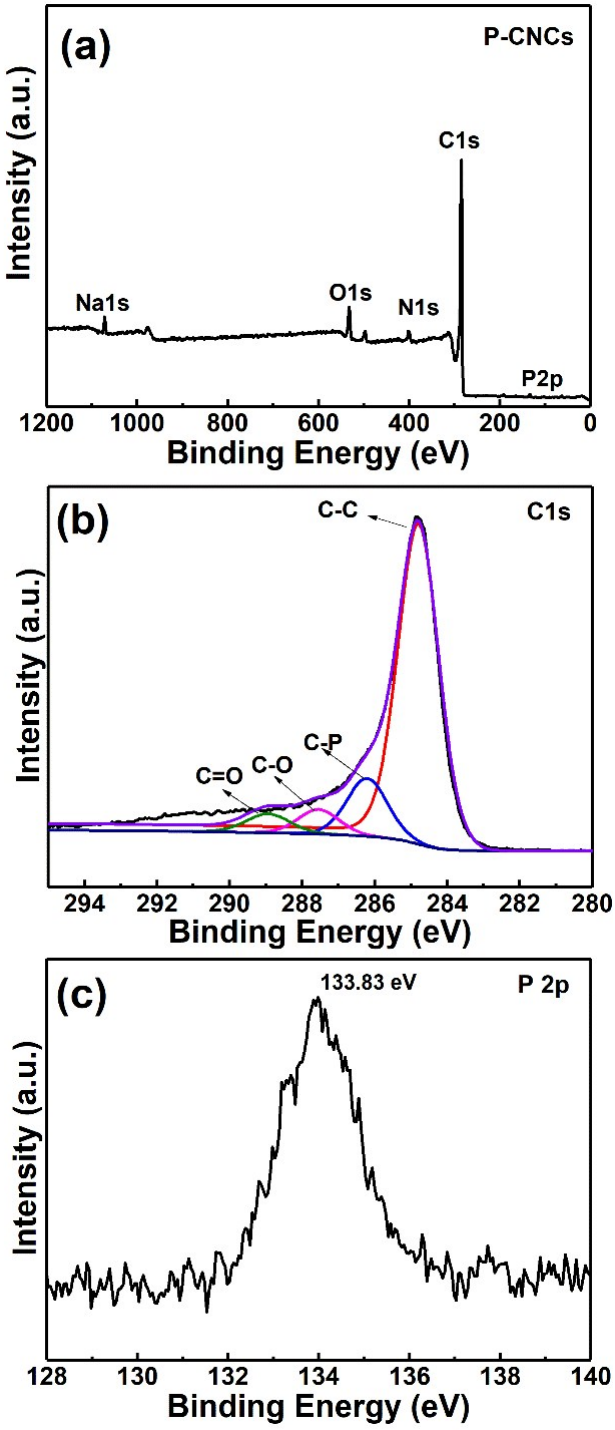

Figure S14 XPS survey scan (a) CNCs, and high resolution spectrum: (b) C 1s and (c) P 2p.

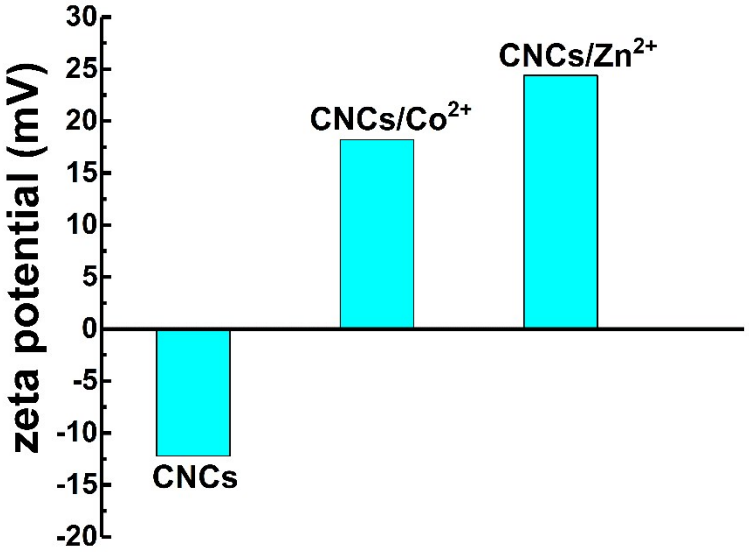

Figure S15 Zeta potential distribution of CNCs, CNCs/Co^{2+}, and CNCs/Zn^{2+}.

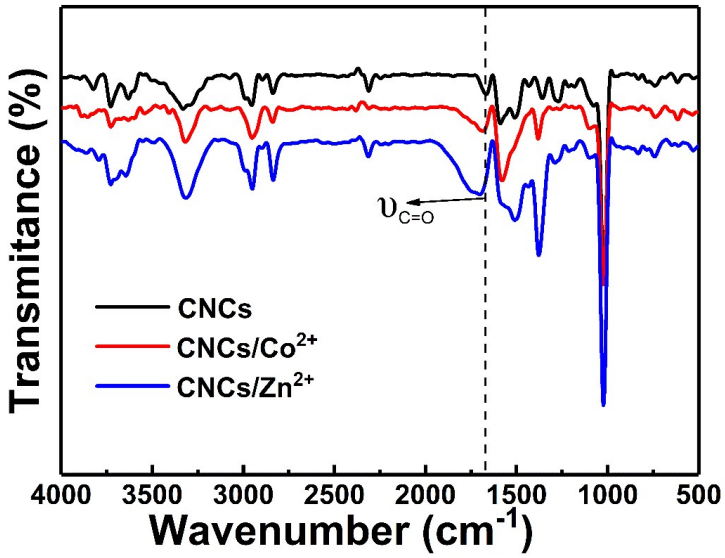

Figure S16 FT-IR spectra of CNCs, CNCs/Co^{2+}, and CNCs/Zn^{2+}.

CNCs/Co^{2+} or CNCs/Zn^{2+} was obtained by immersing CNCs in 1 M metal nitrate dissolved in methanol solution for 6 h followed by several washing with methanol. The zeta potential of CNCs is -12.2 mV. And the zeta potential of CNCs/Co^{2+} and CNCs/Zn^{2+} are 18.2 and 24.4 mV. In Figure S3, the C=O stretching vibration in CNCs, CNCs/Co^{2+}, and CNCs/Zn^{2+} are 1681.8, 1693.4, and 1706.9 cm^{-1}, respectively. The red shift of C=O stretching vibrations of CNCs is attributed to

the electron-withdrawing ability of metal ion. All results demonstrate that the surface deficiency and heteroatom-doped on carbon materials are propitious to adsorb metallic ions.

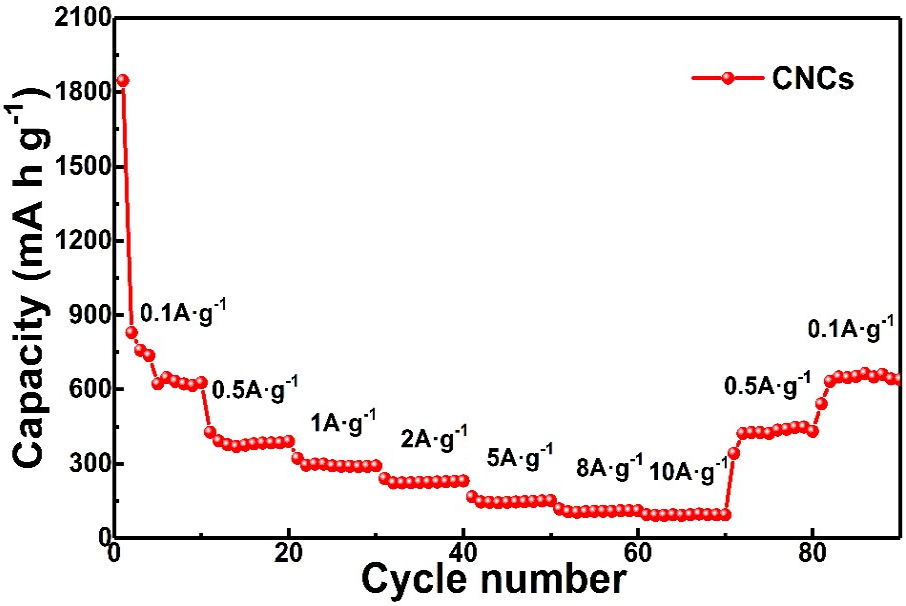

Figure S17 Cycling performance at various current densities of CNCs.

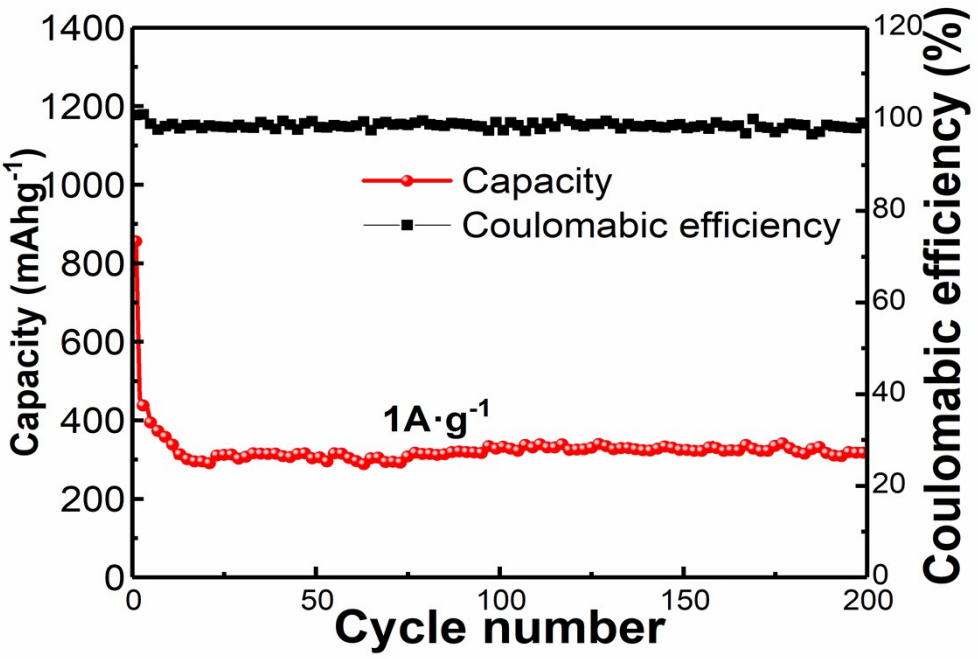

Figure S18 Cycling performance and Coulombic efficiency of CNCs at 1 A g^{-1}.

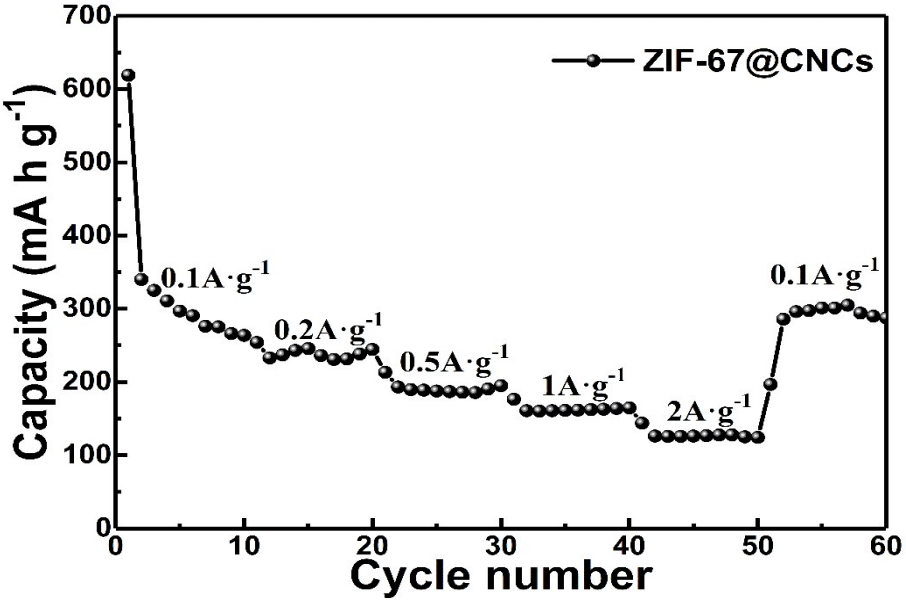

Figure S19 Cycling performance at various current densities of ZIF-67@CNCs.

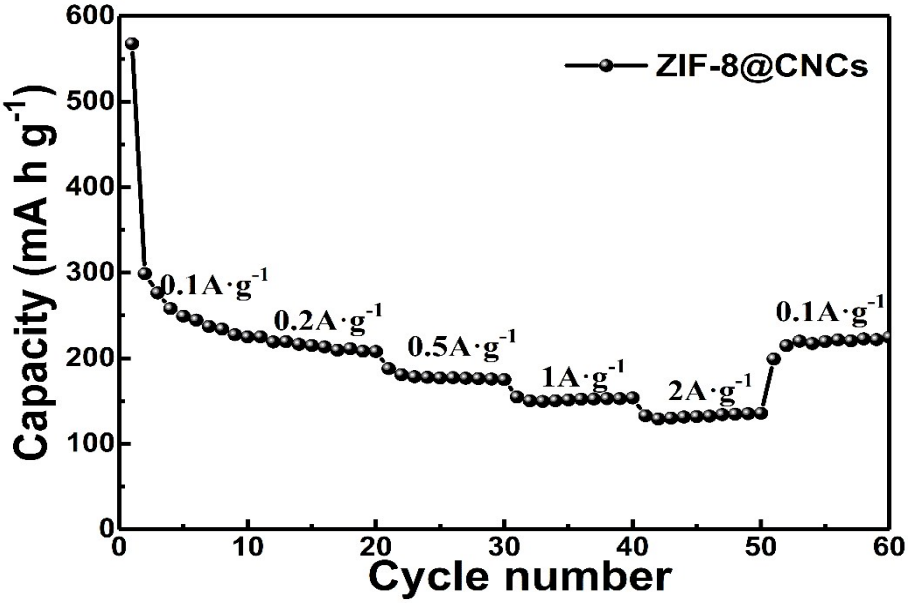

Figure S20 Cycling performance at various current densities of ZIF-8@CNCs.

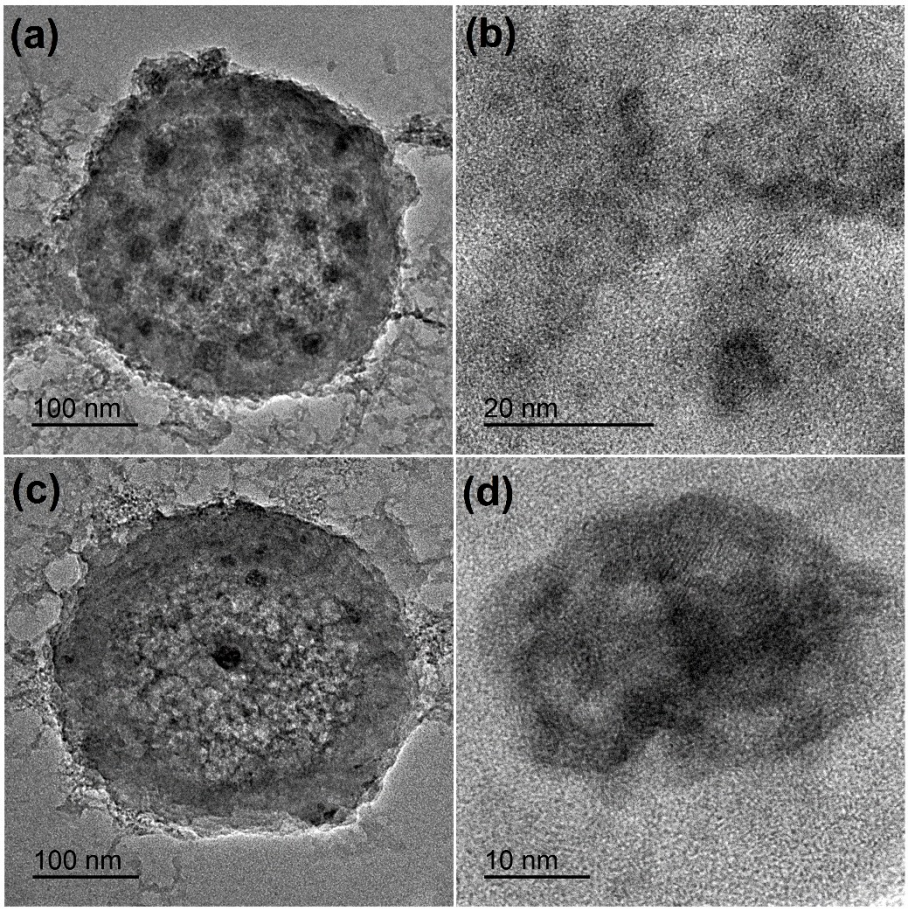

Figure S21 TEM and HRTEM images of (a) (b) CoP@CNCs, (c) (d) ZnP_4@CNCs after 200 cycles at 2 A g^{-1}.

Table S1 Summary of electrochemical performances of different CoP_x-based or ZnP_x-based anodes.

Sample	Rate capability (mA h g^{-1})/ Current density (A g^{-1})	Initial discharge/charge capacity (mA h g^{-1})	Reversible capacity (mA h g^{-1})/ Cycles/Current density (A g^{-1})	Reference
CoP@CNCs	483/5	1200.02/1149.38	1215/1000/0.2 714/500/2	This work
CoP/C nanocomposite	410/0.96	712/531	407/200/1	[1]
CoP nanorods	467/4	956.8/813	894/300/0.5	[2]
1D CoP nanomaterials	215.64/4.4	1564.40/759.61	365/120/3	[3]
CoP/RGO	586/5	2,057/1163	967/200/0.2	[4]
CoP@C-RGO-NF	155/1.6	2455.6/1163.5	473.1/100/0.1	[5]
CoP@C nanorods	384/4.5	1264/963	530/200/1	[6]
Peapod-like CoP HR@rGO	183.3/3.2	1785.4/1196.2	714.7/100/0.1	[7]
CoP nanorod arrays	472/1.6	1067/737	390/900/0.4	[8]
CoP hollow nanoparticle	256/4.45	1556/759	630/200/0.2	[9]
CoP/NC	314.7/1	1045.4/648.6	411.5/2000/0.5	[10]
CoxP-NC	590/1.0	2450/1496	1224/100/0.1	[11]
ZnP_4@CNCs	570/2	1067.1/728.3	773/1000/0.2 462/500/2	This work
ZnP_2/C nanocomposite	200/2	1581/994	350/100/0.1	[12]
ZnP_2 nanowires	300/6.32	1575/1415	1066/500/0.5	[13]
Zn_3P_2 nanowire	700/5	1350/1185	1000/200/0.4	[14]

Refenrence

1 H. T. Kwon, J. H. Kim, K. J. Jeon and C. M. Park, *RSC Adv.*, 2014, **4**, 43227-43234.

2 B. Wang, Q. Ru, Q. Guo, X. Chen, Z. Wang, X. Hou and S. Hu, *Europ. Inorg. Chem.*, 2017, **2017**, 3729-3735.

3 G. Guo, Y. Guo, H. Tan, H. Yu, W. Chen, E. Fong and Q. Yan, *J. Mater. Chem. A*, 2016, **4**, 10893-10899.

4 J. Yang, Y. Zhang, C. Sun, H. Liu, L. Li, W. Si, W. Huang, Q. Yan and X. Dong, *Nano Res.*, 2016, **9**, 612-621.

5 X. Ge, Z. Li and L. Yin, *Nano Energy*, 2017, **32**, 117-124.

6 J. Jiang, C. Wang, W. Li and Q. Yang, *J. Mater. Chem. A*, 2015, **3**, 23345-23351.

7 Z. Han, B. Wang, X. Liu, G. Wang, H. Wang and J. Bai, *J. Mater. Sci.*, 2018, DOI: 10.1007/s10853-018-2143-5, 1573-4803.

8 X. Xu, J. Liu, R. Hu, J. Liu, L. Ouyang and M. Zhu, *Chem.*, 2017, **23**, 5198-5204.

9 D. Yang, J. Zhu, X. Rui, H. Tan, R. Cai, H. E. Hoster, D. Y. Yu, H. H. Hng and Q. Yan, *ACS Appl. Mater. Interfaces*, 2013, **5**, 1093-1099.

10 K. Zhu, J. Liu, S. Li, L. Liu, L. Yang, S. Liu, H. Wang and T. Xie, *Adv. Mater. Interfaces*, 2017, **4**, 1700377.

11 G. Xia, J. Su, M. Li, P. Jiang, Y. Yang and Q. Chen, *J. Mater. Chem. A*, 2017, **5**, 10321-10327.

12 C. M. Park and H. J. Sohn, *Chemistry of Materials*, 2014, **20**, 6319-6324.

13 J.Y. Chen, L.C. Chin, G.A. Li and H.Y. Tuan, *CrystEngComm*, 2017, **19**, 975-981.

14 W. Li, L. Gan, K. Guo, L. Ke, Y. Wei, H. Li, G. Shen and T. Zhai, *Nanoscale*, 2016, **8**, 8666-8672.